photonics

MDPI

Review

Plasmonic Vortices: A Promising Tool Utilizing Plasmonic Orbital Angular Momentum

Zhi Gao [1,2], Dmitri V. Voronine [3] and Alexei V. Sokolov [1,2,4,*]

[1] Department of Physics and Astronomy, Texas A&M University, College Station, TX 77843, USA; zhigao@tamu.edu
[2] Institute for Quantum Science and Engineering, Texas A&M University, College Station, TX 77843, USA
[3] Department of Physics, University of South Florida, Tampa, FL 33620, USA; voronine@usf.edu
[4] Department of Electrical and Computer Engineering, Texas A&M University, College Station, TX 77843, USA
* Correspondence: sokol@tamu.edu

Abstract: An optical vortex (OV) beam is an important type of spatially structured beam. However, the diffraction limit for light with orbital angular momentum (OAM) remains a challenge for certain applications. Surface plasmon polaritons (SPPs) can confine light to nanoscale dimensions and enhance light–matter interactions. Over the past two decades, researchers have begun to explore the imparting of OAM onto SPPs to generate plasmonic vortices (PVs). Since the discovery of PVs, significant efforts have been made in this field, leading to considerable progress. This article reviews these studies in three key areas: (a) the generation and manipulation of PVs, (b) the characterization of PVs, and (c) the application of PVs. We believe that PVs represent a promising tool utilizing plasmonic OAM for both fundamental research and practical applications and hold great potential for the future with continued dedicated efforts.

Keywords: optical vortex (OV); orbital angular momentum (OAM); spin angular momentum (SAM); surface plasmon polariton (SPP); plasmonic vortex (PV); Archimedes spiral (AS); plasmonic vortex lens (PVL)

Received: 24 December 2024
Revised: 17 January 2025
Accepted: 22 January 2025
Published: 31 January 2025

Citation: Gao, Z.; Voronine, D.V.; Sokolov, A.V. Plasmonic Vortices: A Promising Tool Utilizing Plasmonic Orbital Angular Momentum. *Photonics* **2025**, *12*, 125. https://doi.org/10.3390/photonics12020125

1. Introduction

An optical vortex (OV) beam is an important type of spatially structured beam. In 1992, Allen et al. experimentally demonstrated that an optical vortex beam has a well-defined orbital angular momentum (OAM) of $\updownarrow\hbar$ per photon ($\hbar$ is the reduced Planck constant). Such a beam, with its spiral wavefront, can be represented by a spatial profile modified by the factor $\exp(i\updownarrow\theta)$, where θ is the azimuthal angle and $\updownarrow$ is the azimuthal mode index [1], also known as the topological charge. The sign of nonzero $\updownarrow$ determines whether the helical phase in the phase profile is clockwise or anticlockwise, and its helical phase has a singularity at the center, which leads to a donut-shaped intensity profile (Figure 1) [2]. Over the past 30 years, many methods have been developed to generate optical OAM beams, such as mode converters, helical phase plates, fork gratings, phase-type diffraction vortex gratings [3], and metasurfaces [3,4]. Various applications make light with OAM highly attractive, including ultra-large-capacity optical communication, rotating body detection, optical tweezers, laser processing, super resolution imaging [3], directional coupling, and emission via spin–orbital interactions [5], as well as applications in astronomy, metrology, biomedicine and chemistry, quantum entanglement, nonlinear optics, and nanotechnology [6]. Additionally, OAM light is used in the directional excitation

of surface plasmon polaritons (SPPs) [7]. However, the diffraction limit of OAM light remains a challenge for some applications, which can potentially be addressed by SPPs.

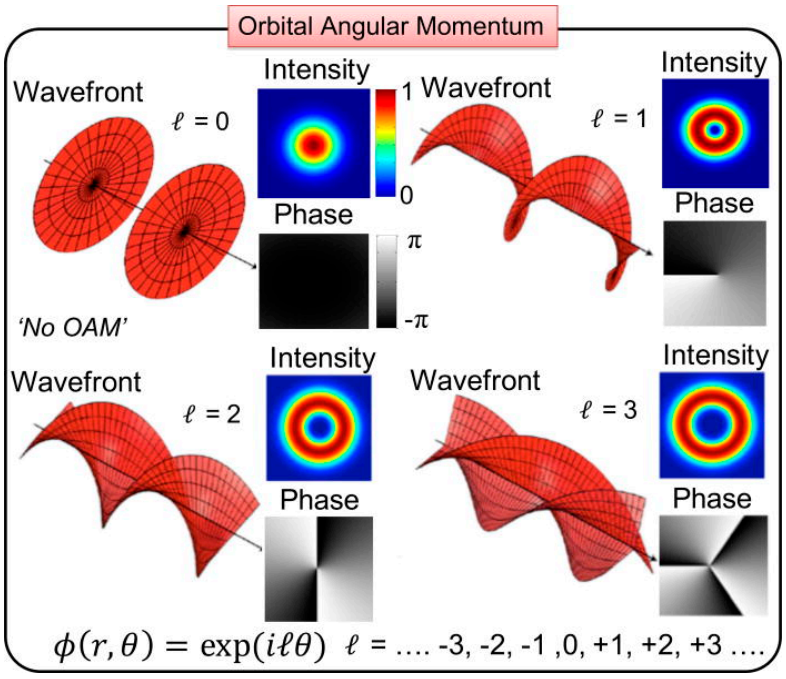

Figure 1. Schematic of OAM beams with different topological charge ↕ values. They exhibit different wavefronts, intensity distributions, and phase profiles. Reprinted from [2]. Creative Commons Attribution (CC BY) license.

SPPs, propagating field-coupled collective electron oscillations at a metal and dielectric interface, can confine fields to nanoscale dimensions and enhance light–matter interactions. Following Ritchie's pioneering work on plasma losses by fast electrons in thin films in 1957 [8], much attention has been devoted to SPPs and numerous applications have emerged alongside the development of nanotechnology over the past decades. These applications include plasmonic solar cells [9,10], medical diagnoses [11], chemical reactions [12], biosensors [13,14] and other sensors [15], molecular electronics [16], meta-optics [17], waveguides [18], and color generation [19], among others. Among these, plasmon-enhanced Raman and fluorescence techniques, such as surface-enhanced Raman spectroscopy (SERS) and tip-enhanced Raman spectroscopy (TERS), have gained prominence and now play a vital role in many areas of research. In plasmon-enhanced Raman and fluorescence, surface plasmons are crucial, as they can highly confine and significantly enhance electric fields [20]. This has led to a greatly improved detection sensitivity and has paved the way for numerous applications since the discovery of the effect [21–27].

However, it was not until the past two decades that researchers began to explore the imparting of OAM onto SPPs to generate plasmonic vortices (PVs). PVs are evanescent Bessel excitations that also possess OAM. But unlike free-space optical vortices (OVs), PVs are generated by surface plasmons, giving them the advantages of field confinement and enhancement in addition to the properties of OAM. Since the discovery of PVs [28,29], significant efforts have been made in this field, leading to considerable progress. In this review, we cover these works in three key areas: (a) the generation and manipulation of PVs; (b) the characterization of PVs; and (c) the application of PVs.

2. Generation and Manipulation of Plasmonic Vortices

Since PVs have gained researchers' attention [28], various plasmonic structures and methods have been proposed to realize PVs. The commonly used method among them is

the Archimedes spiral (AS) [28,30]. However, to generate localized vortices with multiple topological charges in a single structure, several variations of this spiral structure have emerged [30–34]. In this section, we review some work on the generation and manipulation of PVs.

2.1. Direct Transformation from Optical Vortices to Plasmonic Vortices

It is intuitive to see that the chirality of incident light is preserved in the evanescent Bessel beam through the symmetrical structure [28]. Shutova et al. proposed that a nanolens could efficiently focus OVs to the nanoscale and generate PVs (Figure 2) [35]. Meanwhile, Sunaba et al. demonstrated that a tailored plasmonic multimer could confine the Laguerre–Gaussian (LG) mode field into a nano-sized gap by transferring high-order OAM and spin angular momentum (SAM) from photons to localized plasmons [36].

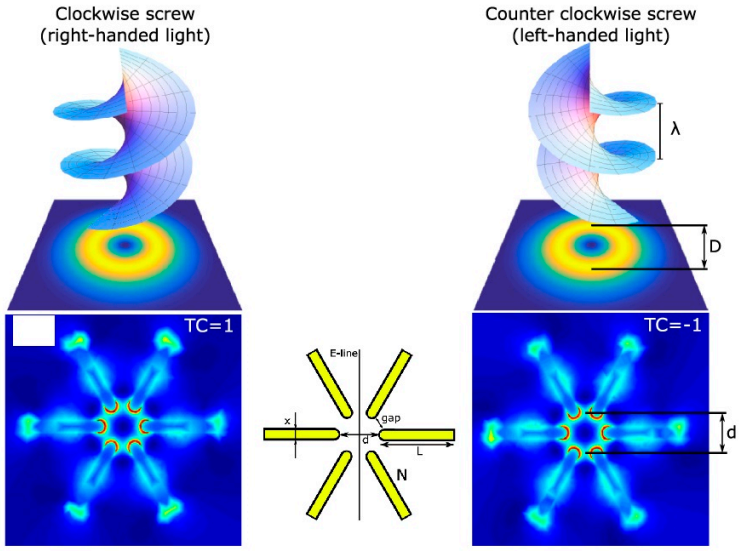

Figure 2. Schematic of a nanolens and its field confinement for OAM light. Adapted with permission from [35]. © 2022 Astro Ltd.

2.2. Modified Archimedes Spirals or Other Methods

One commonly used method to generate PVs is the AS, whose trajectory is given by $r = r_0 + \frac{\varphi+\pi}{2\pi} m\lambda_{spp}, \varphi \in (-\pi,\ \pi]$, where r_0 is the initial radius, λ_{spp} is the wavelength of excited surface plasmons, φ is the azimuthal angel, and m is an integer (Figure 3a) [37]. Both the path difference of the spiral contour inducing the dynamic phase and the polarization of excitation light determine the value of plasmonic OAM [33]. To overcome the limitation of generating PVs with multiple charges in a single structure, various modifications have been introduced, such as a segmented AS [31,32]. Tan et al. achieved an arbitrary combination of OAM numbers by simultaneously manipulating both geometric and dynamic phases in a phase gradient spiral lens [31]. Similarly, Zhang et al. demonstrated that the superposition of two different OAM states could be attained and altered in a single generator by adjusting these two phases (Figure 3b,c) [32]. Tsai et al. overcame the spin-locked OAM generation restriction, enabling spin-independent OAM generation by incorporating the geometric phase with the dynamic phase [30]. Zang et al. were able to control terahertz (THz) near-field PVs with multiple degrees of freedom by combining the geometric and dynamic phases [33]. Furthermore, they introduced an approach to generate multiplexed THz PVs using geometric metasurfaces [38]. Prinz et al. proposed the possibility of achieving arbitrarily large plasmonic OAM values by modifying the helicity of the incident light and tailoring both the local and global geometries of vortex generators [34].

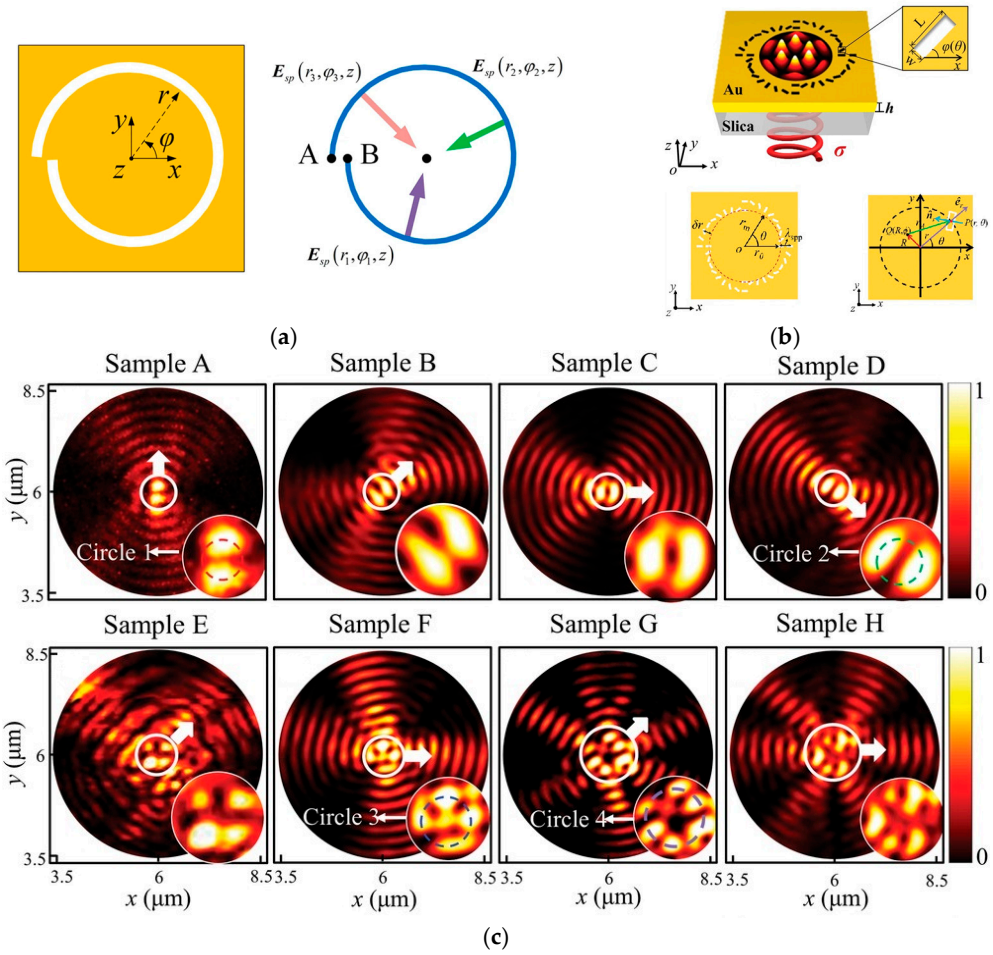

Figure 3. Archimedes spirals and modified ASs. (**a**) Schematic of an AS and the excitation of PVs. Reprinted from [37]. Copyright © 2016, The Author(s). Creative Commons Attribution 4.0 International License. (**b**) Schematic of a segmented spiral metasurface, whose rotation angle of the slits is $\phi(\theta) = q\theta + \alpha_0$ and the radius of the spiral is $r_m = initial\ radius + \lambda_{spp} \times \frac{mod(m\theta,\ 2\pi)}{2\pi}$, where θ is the azimuthal angle, q is the rotation order of the slits, m is the geometric order of the spiral, α_0 is the initial angle of the slits, λ_{spp} is the SPP wavelength, and $mod(m\theta,\ 2\pi)$ represents the remainder of the division of $\frac{m\theta}{2\pi}$. (**c**) Near-field intensity measurements for the metasurface samples A–H interacting with right circularly polarized light, varying three parameters: q, m, and α_0. Adapted with permission from [32]. © 2019 WILEY-VCH Verlag GmbH & Co. KGaA, Weinheim.

Additionally, some studies have utilized added degrees of freedom in the light source to manipulate PVs. Wang et al. proposed a technique for dynamically sculpturing PVs from integer to fractional OAM by leveraging the radial phase gradient induced by the propagation of an incident LG beam [37]. Huang et al. proposed a lens capable of generating PVs with linearly polarized light [39]. Bai et al. demonstrated a wavelength-tunable PV generator that can control both the topological charges and the vortex locations [40]. Recently, Gu et al. showed that positively elliptically polarized beams can excite SPP vortices with a relatively uniform electric field intensity distribution, avoiding the effect of amplitude ratio variations in the beam. This new plasmonic lens also allows the modulation of topological charges using vector beam illumination [41].

Even with other structures, researchers have achieved PVs. Yuan et al. localized electromagnetic vortex waves with multimodal topological charges, creating a PV printing technology using a periodic array of metaparticles (Figure 4a) excited by coplanar waveguide-based spoof SPPs [42]. Xu et al. proposed a design that selectively controls the conversion from optical SAM to plasmonic OAM through near-field coupling between

paired resonators in a metasurface (Figure 4b) [43]. Gu et al. introduced a PV lens based on the geometric phase (Figure 4c), capable of generating SPP vortices when illuminated by either circularly or linearly polarized light [44]. Additionally, Triolo et al. confirmed that vortex modes can be generated in an elliptical nanohole when illuminated by incident light with a polarization direction differing from the ellipse's axes [45]. Furthermore, Ghanei et al. advanced this approach using metal–insulator–metal structures (Figure 4d), producing uniform, high-quality PVs with varied topological charges by smoothly adjusting the ellipse's minor-to-major axis ratio [46].

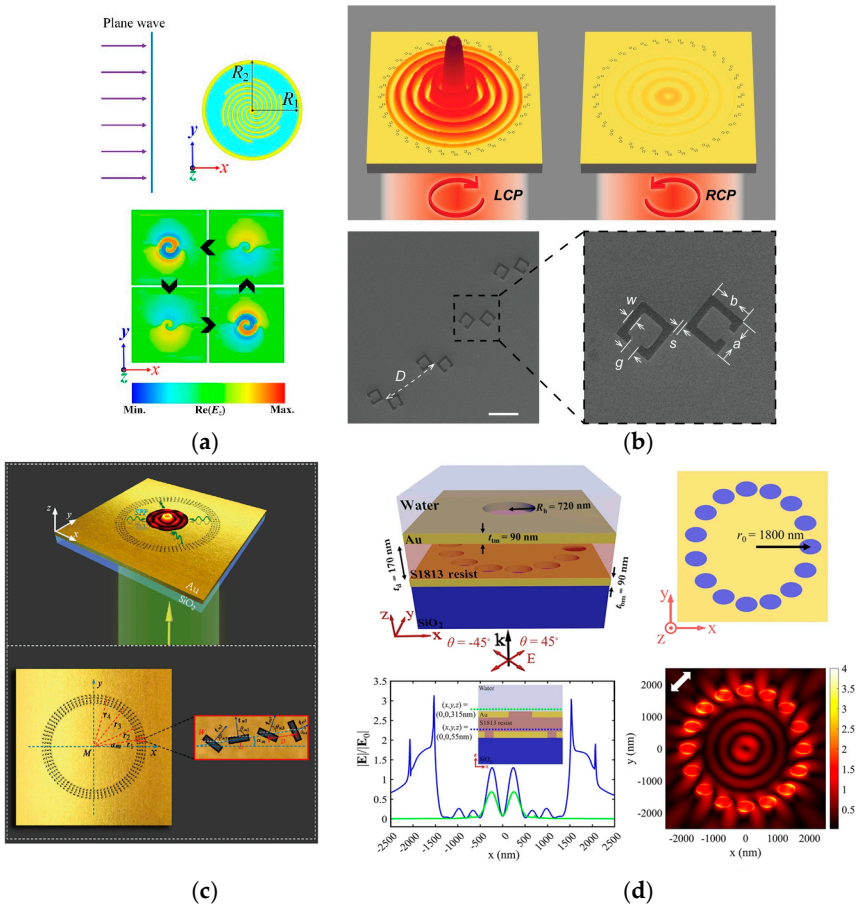

(**a**) (**b**) (**c**) (**d**)

Figure 4. Schematic of various plasmonic vortex generation structures. (**a**) A six-long-spiral meta-particle and four snapshots showing the real-time evolution of the near-field distribution of the E_z component, excited by a linearly polarized plane wave at 8.5 GHz. Adapted with permission from [42]. © 2021 Wiley-VCH GmbH. (**b**) A metasurface of ring-shaped paired resonators. Reprinted with permission from [43]. © 2019 WILEY-VCH Verlag GmbH & Co. KGaA, Weinheim. (**c**) A meta-atom comprising four rectangular slits arranged along a circular contour. Reprinted from [44]. © 2023 Optica Publishing Group under the terms of the Optica Open Access Publishing Agreement. (**d**) A metal–insulator–metal structure featuring a circular array of elliptical holes embedded in the bottom gold film and a central circular hole in the top gold film, along with its normalized electric field distribution in the XY plane and along the X-axis. Adapted from [46]. Copyright © 2023, The Author(s). Creative Commons CC BY license.

2.3. Spatiotemporal Dynamics/Modulation of Plasmonic Vortices

It is widely assumed that static boundary conditions and specific excitations determine the generated field. However, the initially generated PV evolves over time due to various factors, such as the propagation and reflection of the SPPs and spin–orbit coupling between light and the SPPs. Consequently, the spatiotemporal dynamics of PVs, alongside their average field distribution, are crucial for understanding the mechanism underlying these

physical processes and expanding their range of applications. Here, we highlight some important studies that offer insight into these dynamics. Yang et al. counterintuitively identified the surprising existence of multiple deuterogenic PVs in a single plasmonic vortex lens (PVL), even when excited by a fixed, circularly polarized vortex beam, providing a glimpse into the dynamics of PVs [47]. Spector et al. explained that the reflection of the SPP vortex from structural boundaries generates successive vortex pulses with increasing topological charges as a function of time (Figure 5a) [48]. Subsequently, Yuan et al. demonstrated that PVs can have distinct spatiotemporal dynamics based on different coupler designs, even when the vortices possess the same topological charge (Figure 5b) [49]. Furthermore, Yuan et al. verified the existence of a temporally deuterogenic vortex mode whose spatiotemporal evolution could be tailored through various PVL designs and incident beams, enriching our understanding of PV dynamics [50]. Li et al. explored the effects of spin−orbit coupling on the spatiotemporal modulation of ultrafast PVs, including the formation of multiple phase singularities, energy flow loops, and changes in the localized OAM/SAM distribution [51].

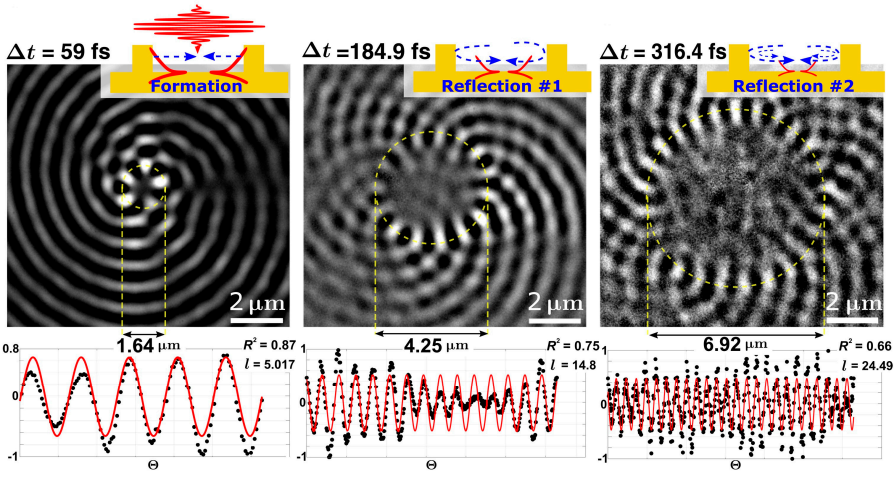

(**a**)

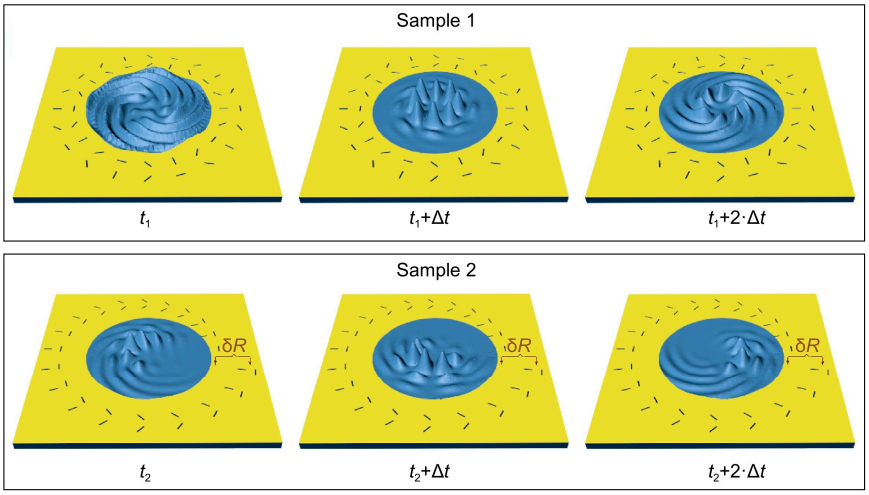

(**b**)

Figure 5. Spatiotemporal dynamics of plasmonic vortices. (**a**) Revolution stages of a vortex, from its generation to after the first and second reflections at the boundary. The bottom lines show azimuthal and radial fitting of the diameter and the number of lobes in the main vortex signal. Adapted from [48]. Copyright © 2021, The Authors, some rights reserved. Creative Commons Attribution License 4.0 (CC BY). (**b**) Schematic of distinct generation and evolution behaviors of vortices with the same topological charge, produced by different couplers. Reprinted from [49]. © The Author(s) 2023. Creative Commons Attribution 4.0 International License.

3. Characterization of Plasmonic Vortices

Several methods have been developed to probe plasmonic local fields generated by SPPs since their discovery. The most popular technique is scanning near-field optical microscopy (SNOM), which can operate in both apertured and apertureless modes. Additionally, some modifications have been applied to enhance its performance. For instance, Michaelis et al. attached a nanoscopic active medium to the SNOM tip to increase its spatial resolution [52]. Another method is a photon scanning tunneling microscope (PSTM), in which SPPs are excited by the reflection of an evanescent light field at the metal–glass interface in the Kretschmann configuration. Krenn used a PSTM to experimentally observe the near-field optical effects of Au nanoparticles [53]. Sandtke et al. reported the observation of slow and femtosecond SPP wavepackets using a phase-sensitive, time-resolved PSTM [54].

Two-photon luminescence microspectroscopy (TPLM) is another approach, and Ghenuche et al. used it to resolve the resonant spectra map of gap antennas [55]. Moreover, Lahiri et al. used the photothermal-induced resonance (PTIR) technique to identify the dark plasmonic resonance of gold asymmetric split-ring resonators (A-SRRs) [56]. Lastly, Stockman et al. proposed the combination of photoelectron emission microscopy (PEEM) with attosecond streaking spectroscopy to study the dynamics of plasmons with a nanometer and attosecond spatiotemporal resolution [57]. Here, we summarize some studies on the characterization of PVs.

3.1. Detection of Plasmonic Vortices

Gorodetski et al. observed the circular, polarization-dependent, near-field intensity distribution of a spiral plasmonic structure with SNOM [29]. Later, Carli et al. demonstrated different OAM states of the PV by detecting the "on" and "off" status of four gold nanorods placed in a hole at the center of the spiral using SNOM (Figure 6a) [58]. Yang et al. further revealed the existence of multiple PVs within a single PVL excited by a fixed, circularly polarized vortex beam and demonstrated general spin-to-orbit coupling [47]. However, the above studies utilized monochromatic global excitation to achieve spatially resolved detection. To characterize the dispersion of locally excited PVs, Hachtel et al. investigated the cathodoluminescence response generated by the excitation of a fast electron beam in a scanning transmission electron microscope (STEM), allowing for an examination of the plasmonic phase and amplitude across a broad spectral range simultaneously (Figure 6b) [59].

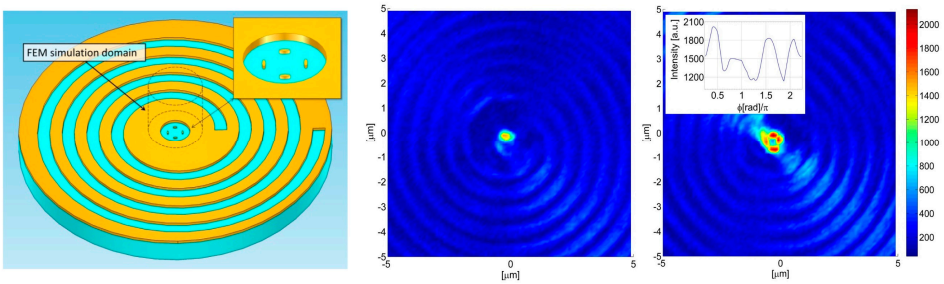

(**a**)

Figure 6. *Cont.*

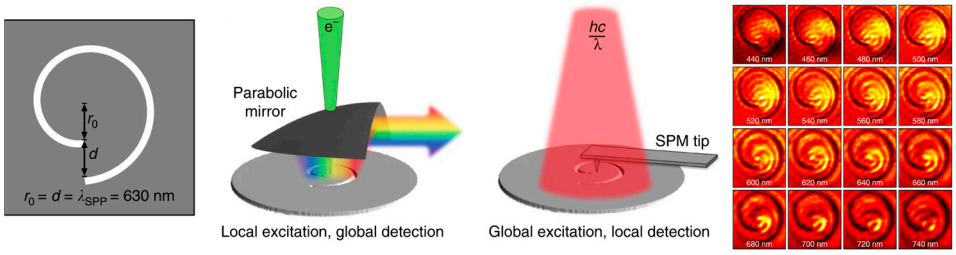

(**b**)

Figure 6. Plasmonic vortex detection. (**a**) Structure of a plasmonic lens with four nanorods at its center. The "on" and "off" states of these rods under the SNOM scan indicate the OAM states of PVs. Adapted with permission from [58]. © 2014 Optical Society of America. (**b**) Schemes of measuring dispersion in PVs. The cathodoluminescence of PVs, generated by the interaction of a fast electron beam of a scanning transmission electron microscope, enables the simultaneous measurement of their phase and amplitude across a broad spectral range. Adapted from [59]. © The Author(s), 2019. Creative Commons Attribution 4.0 International License.

3.2. Dynamics Detection of Plasmonic Vortices

Next, we reviewed work on the detection of the dynamics of PVs, which helped to unveil the nature of plasmonic angular momentum and expanded the possibilities for new applications. Spektor et al. observed the detailed spatiotemporal evolution of nanovortices using time-resolved, two-photon photoemission electron microscopy (TR-2P–PEEM) and extracted the OAM magnitude of light based on the angular velocity of the vortex (Figure 7a) [60]. Additionally, Spektor et al. successfully achieved optical spin–orbit mixing through the interaction between three-dimensional (3D) light and two-dimensional (2D) PVs, with its mixing outcome transferred to matter via the excitation of electrons through a two-photon absorption process. The electrons were collected to provide a high-resolution map of the interaction (Figure 7b) [61].

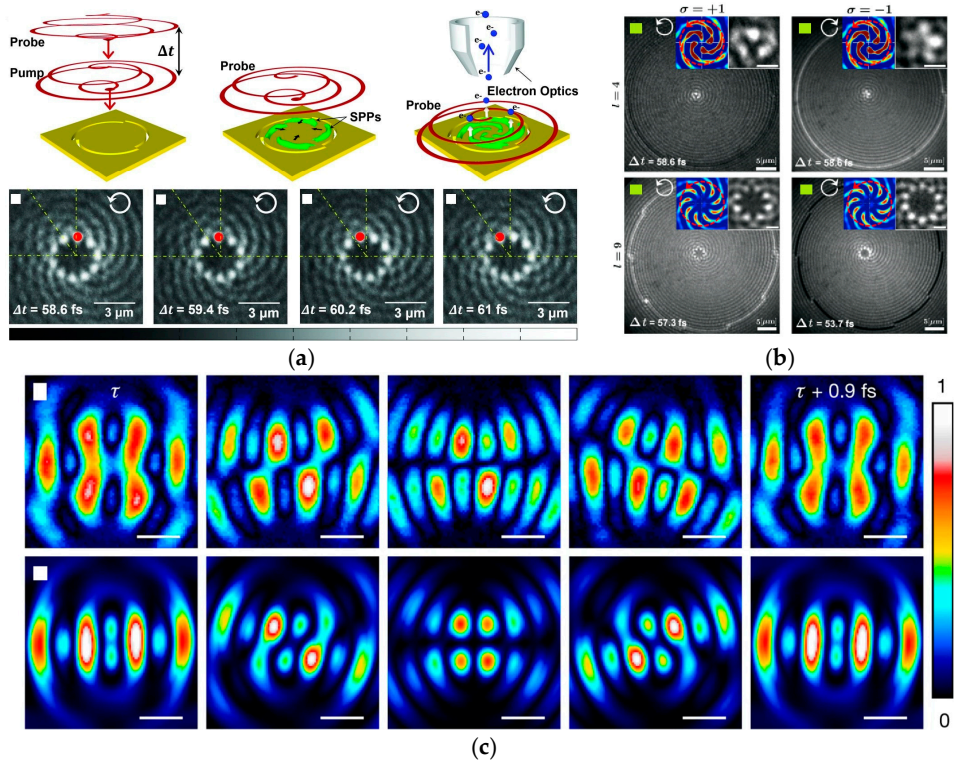

Figure 7. Dynamics detection of PVs. (**a**) Schematic of time-resolved, two-photon photoemission electron microscopy for detecting the revolution stage of PVs within a single optical cycle of ~2.67 fs.

Reprinted with permission from [60]. © 2017, American Association for the Advancement of Science. (**b**) Simulated and experimental results showing spin–orbit mixing of light with PVs. Reprinted from [61]. Creative Commons Attribution 4.0 International License. (**c**) Attosecond-resolved videos depicting the spatial evolution of vortex fields, captured using ultrafast nonlinear coherent photoelectron microscopy (top) and simulated (bottom). The color scale represents photoelectron counts. The white scale bars are SPP wavelength, 530 nm. Adapted with permission from [62]. © The Author(s), under exclusive license to Springer Nature Limited 2020.

Meanwhile, Tsai et al. proposed a paradigm where the dynamic phase is incorporated with the geometric phase, allowing for the controllable production of both spin-dependent and -independent OAM, enabling the study of OAM formation dynamics without spin hybridization [30]. Dai et al. captured videos of the spatial evolution of vortex fields in an Archimedean coupling structure using ultrafast nonlinear coherent photoelectron microscopy (Figure 7c), revealing that some vortices are generated through spin–orbit interactions, forming spin textures known as plasmonic meron quasiparticles through three of these vortices [62].

The aforementioned studies focused on the integer OAM of plasmonic vortices. However, Bauer et al. used TR-2P−PEEM and near-field optical microscopy to measure and analyze the time evolution of fractional OAM SPPs, revealing that their fields depend on integer OAM eigenstates [63].

4. Applications of Plasmonic Vortices

By leveraging the properties of the local fields of SPPs and their OAM, PVs offer several advantages for various applications. Below, we summarize some areas where PVs show promise, underscoring their potential as valuable tools for future research.

4.1. Tip-Enhanced Raman Spectroscopy Based on Spiral Plasmonic Lens Excitation

Unlike the far-field light excitation used in conventional TERS, TERS based on a spiral plasmonic lens excites the tip using SPPs generated by the symmetry-breaking lens. This approach creates a strong longitudinal electric field at the focus [64], resulting in a higher excitation efficiency of the near-field Raman signal and reduced far-field background noise, thereby enhancing the detection sensitivity [65]. Although this detection method is limited by its ability to detect only samples positioned at the center of the plasmonic lens (where the SPP field is concentrated), improvements can be made to address this limitation. For example, Gu et al. theoretically demonstrated that, by rotating the plasmonic lens and adjusting the incident angle of circularly polarized light, the focus position can be shifted within the lens, enabling sample scanning for imaging [66].

4.2. Chirality Detection

Since the discovery of OVs, many efforts have been made to utilize twisted light to discriminate chiral molecules, as the OAM in an OV can take unlimited values compared to the SAM, which has only two defined values. Currently, circular dichroism using circularly polarized excitation and the optical rotation of linearly polarized light are primary methods for characterizing chirality. Although some studies have shown that twisted light does not achieve chiral differentiation through electric or magnetic dipole interactions [67], recent experiments have demonstrated that linearly polarized twisted waves can exhibit helical dichroism when interacting with chiral samples via higher-order interactions, such as electric quadrupole interactions (Figure 8a,b) [67,68].

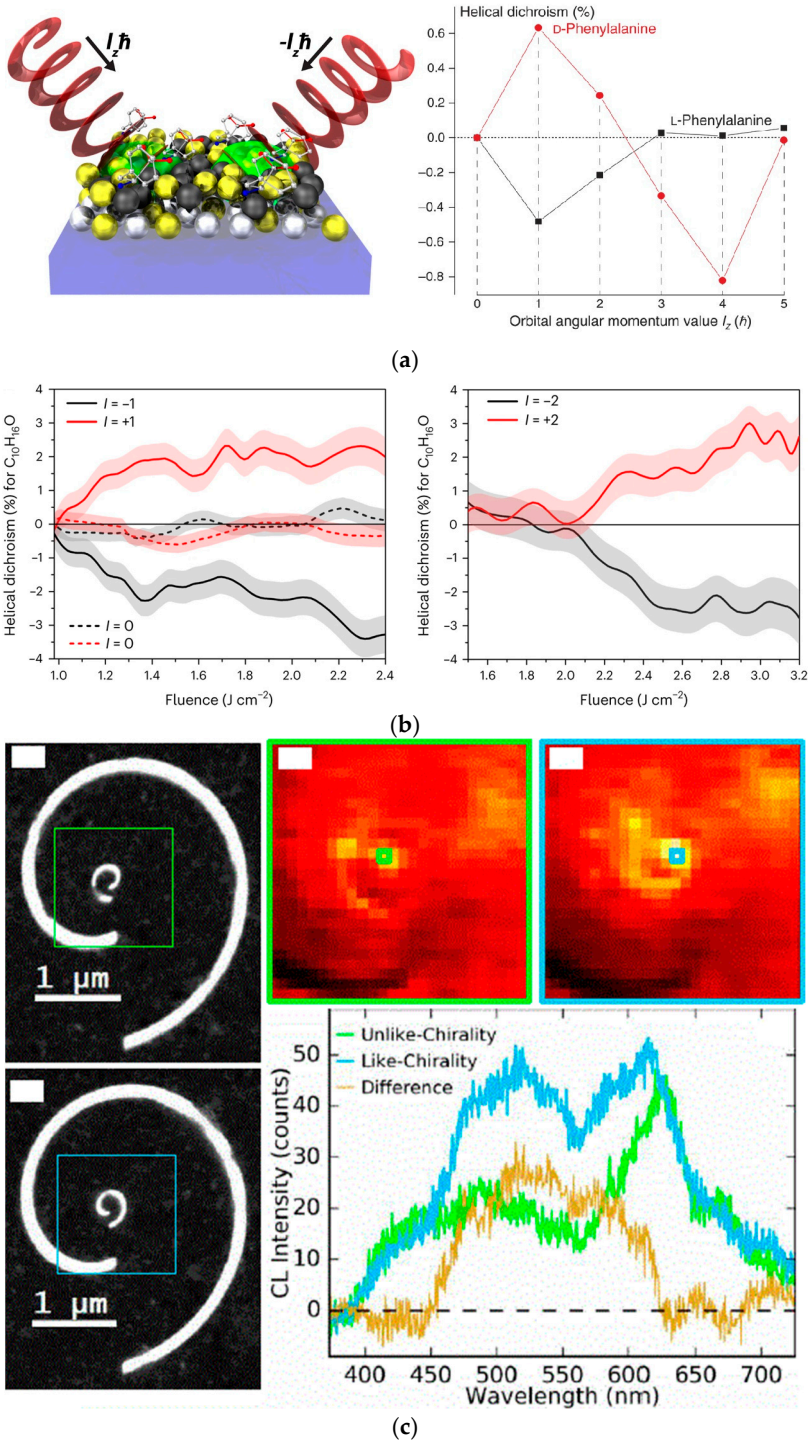

Figure 8. Chirality detection using optical or plasmonic vortices. (**a**) Helical dichroism through optical vortices interacting with enantiomers via strong electric quadrupole fields. Reprinted with permission from [67]. Copyright © 2016, The Authors. (**b**) Helical dichroism in fenchone using linearly polarized light, where $l = 0$ represents Gaussian beams and $l = \pm 1$, 2 represents vortex beams. Reprinted with permission from [68]. © The Author(s), under exclusive license to Springer Nature Limited 2022. (**c**) Chirality detection with plasmonic vortices, showing that like-chirality nanospirals exhibit stronger cathodoluminescence intensities than unlike-chirality nanospirals. Reprinted with permission from [69]. © 2017 Optical Society of America.

Specifically, Begin et al. used femtosecond high-power laser excitation to explore the helical dichroism effect arising from the coupling of the electric dipole and electric quadrupole terms [68]. Similarly, Burllot et al. leveraged the local fields of nanoparticle

aggregates to enhance the engagement of OAM with molecular chirality through electric quadrupole fields (EQFs) [67]. These findings suggest that nanoplasmonic vortices, with their enhanced fields, could potentially discriminate enantiomers via high-order transition moments. Additionally, Hachtel et al. observed that nanospirals positioned at the center of a vortex plasmon generator showed a greater cathodoluminescence when their chirality matched that of the generator (Figure 8c) [69].

4.3. Circular Polarization Analyzer

Numerous studies have demonstrated that plasmonic metasurfaces can manipulate the polarization of incident light through SPPs. OVs can even be generated using specifically designed plasmonic structures by specific incident polarization [70]. In recent years, researchers have shown that a spiral plasmonic lens can focus an appropriate circularly polarized light into a PV. Moreover, left- and right-handed circularly polarized light is focused into spatially separated plasmonic fields by such a lens (Figure 9). Zhan et al. utilized this property to create an efficient miniature circular polarization analyzer [71,72]. Zhang et al. proposed a more complex coaxial AS structure, and their simulation results indicated an improved coupling efficiency as a circular polarization analyzer [73]. Additionally, Afshinmanesh et al. integrated linear and spiral slits to measure the polarization state with the complete Stokes parameters [74,75].

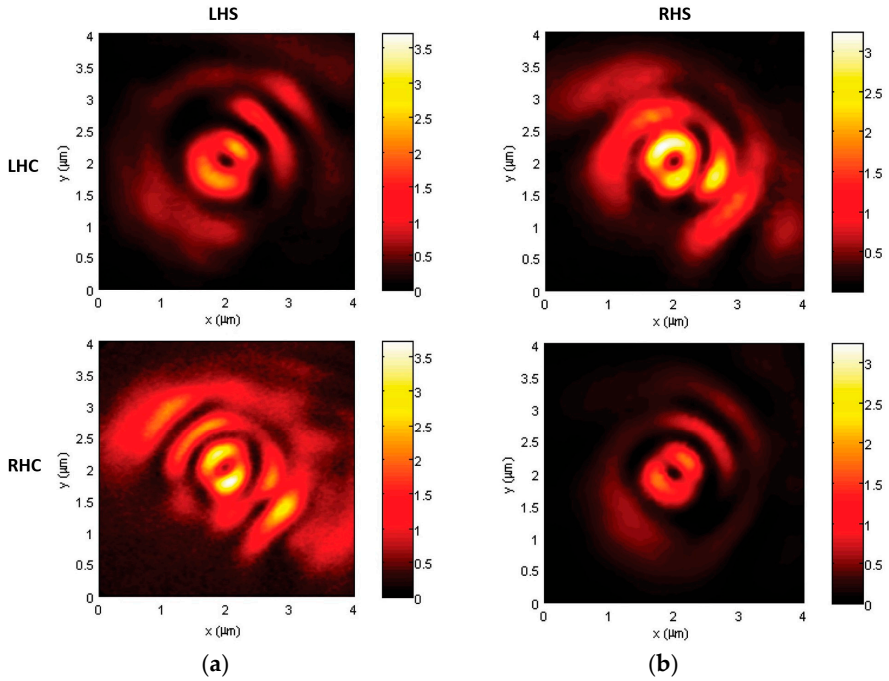

Figure 9. SNOM images of a (**a**) left-handed and (**b**) right-handed single Archimedean spiral slot (LHS) under left-handed circular (LHC) and right-handed circular (RHC) polarization illumination, showing that a specific spiral has different focusing behaviors for two circular polarizations. Reprinted with permission from [71]. Copyright © 2010 American Chemical Society.

4.4. Generation and Readout of Optical OAM

Not only can OVs generate PVs, but PVs can also be used to generate OVs. This section briefly reviews some studies on OV generation using PVs, focusing on two main methods: (1) A tapered metal tip surrounded by a spiral slit, where the PVs generated by the spiral structure are coupled into free space via the metal tip at the center (Figure 10a) [76–78]. (2) A PVL with a central hole, where PVs produced by the PVL transmit through the hole and scatter at its edge into free space [79]. Additionally, modifications to the second

method include positioning the spiral lens and the hole on two separate metal layers with an insulating layer in between. This design prevents impinging light from directly transmitting through the hole, resulting in a pure OAM state (Figure 10b) [80].

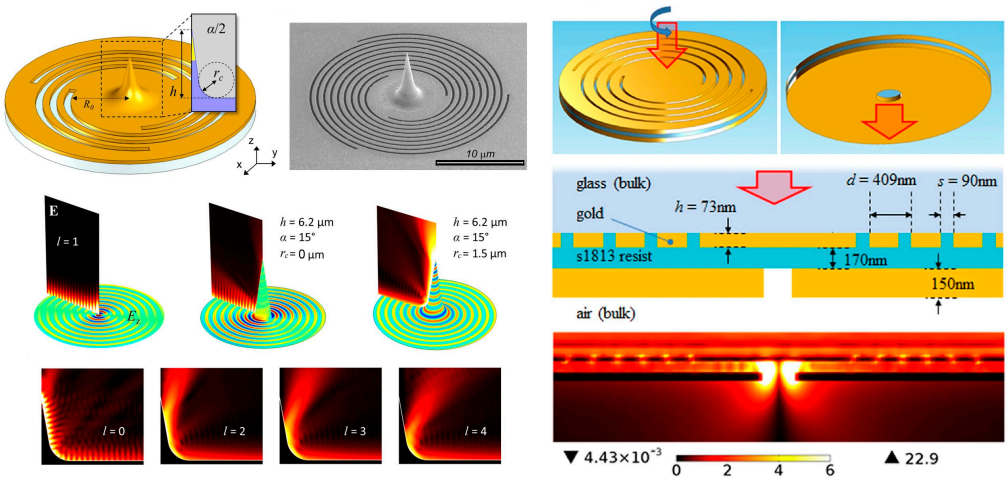

(**a**) (**b**)

Figure 10. Generation of optical OAM. (**a**) Structure of a tapered gold tip surrounded by a spiral slit for generating optical vortices. The right two |E| maps in the middle row show that the same tip with different basis curvature radii r_c has different far-field coupling effects. The |E| maps at the bottom show the far-field coupling effect of the same tip for PVs with different topological charges l. Reprinted from [76]. © 2016 American Chemical Society. Creative Commons license CC BY-NC-ND 4.0. (**b**) Metal–insulator–metal holey plasmonic vortex lens used to generate optical vortices. Reprinted from [80]. Copyright © 2016, The Author(s). Creative Commons CC BY license.

Furthermore, although Prinz et al. reviewed some works on employing a PVL for demultiplexing OAM at a chip scale [81], additional studies are included here as well. Wang et al. proposed an elliptical AS that is illuminated by incident light with different angular momenta, generating various PVs. The positions and sizes of these PVs can provide information about both the spin and orbital angular momentum of the incident light simultaneously (Figure 11a) [82]. Using a circular plasmonic lens, Liu et al. established interference between the surface plasmon and directly transmitted light. The rotation direction and amount of rotation of these interference patterns are linked to the sign and value of the OAM, respectively (Figure 11c) [83]. Mei et al. proposed a semi-ring plasmonic nanoslit that can focus various OAM modes of light onto spatially separate positions on the metallic surface. Additionally, they enhanced the focal intensity by increasing the number of such semi-ring nanoslits concentrically (Figure 11b) [84].

4.5. Plasmonic Vortex Interferometers

Interferometers are commonly used tools in both research studies and commercial applications. Lang et al. proposed a novel interferometer that utilizes the interference between customized PVs, enabling the measurement of the polarization state, spin, and orbital angular momentum of incident light. The core component is the versatile design of the PVL, which consists of two sets of slit resonators, varying the separation distances and orientation angles on the two circular contours, and features multiple degrees of freedom that allow for the independent designation of the phase, relative amplitude, topological charge, and number of PVs generated by two orthogonal circular polarizations (Figure 12) [85].

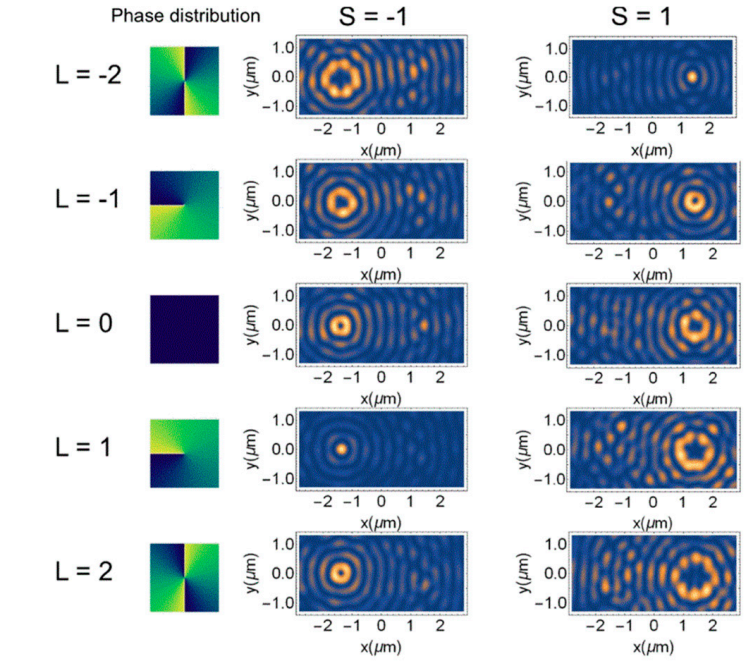

(**a**)

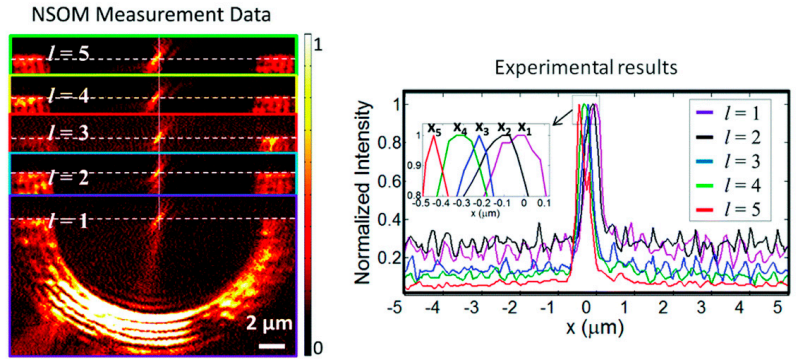

(**b**)

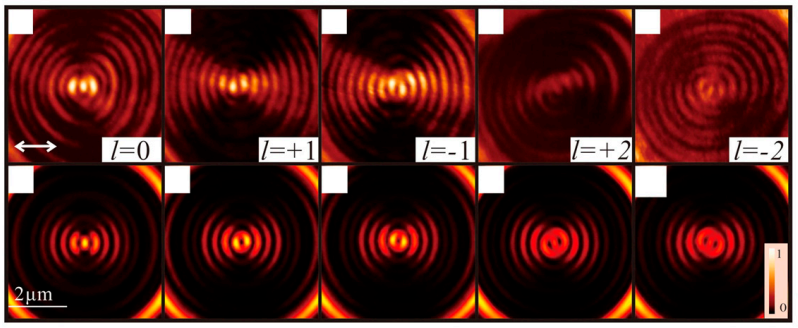

(**c**)

Figure 11. Readout of optical OAM. (**a**) Positions and sizes of PVs in an elliptical AS reveal both the spin and orbital angular momentum of light. Reprinted from [82]. IEEE Open Access Publishing Agreement (OAPA), 1943-0655 © 2017 IEEE. (**b**) Semi-ring plasmonic nanoslits capable of focusing various OAM modes of light onto spatially distinct positions. The right figure depicts intensity profiles along the white dashed lines in the left figure. Adapted with permission from [84]. © The Royal Society of Chemistry 2016. (**c**) Circular plasmonic lens that utilizes interference between plasmon and transmitted light to identify OAM states of light, causing different intensity distributions, shown experimentally (top) and computationally (bottom). Reprinted with permission from [83]. Copyright © 2013, The Author(s).

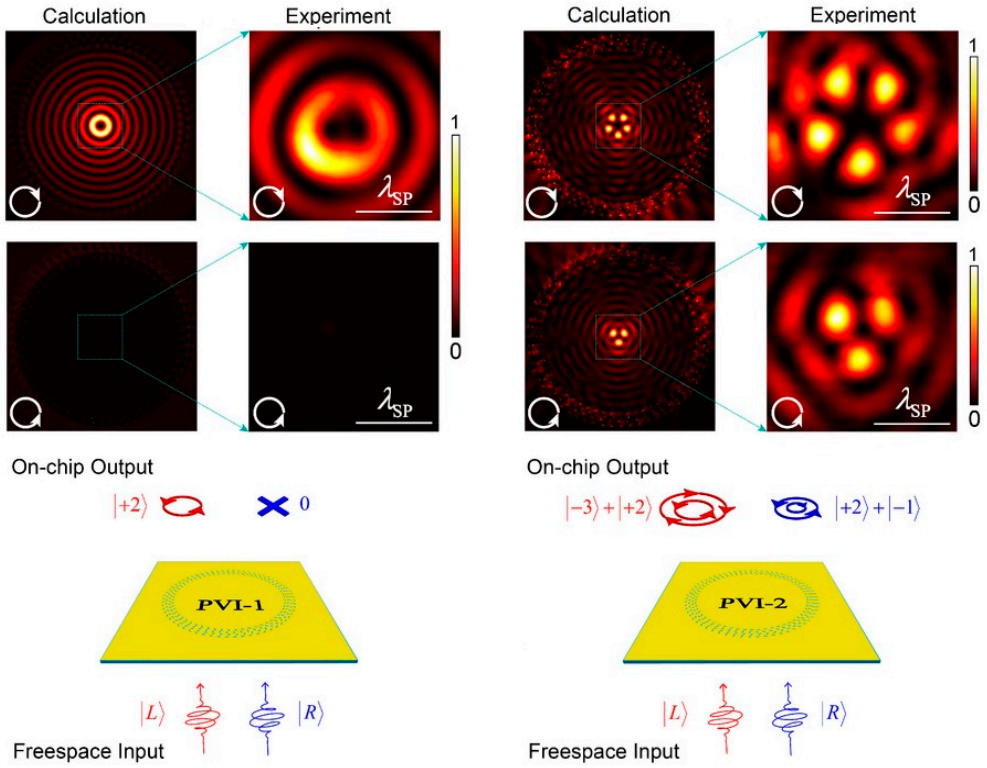

Figure 12. Plasmonic vortex interferometers (PVIs). Interferometers PVI-1 and PVI-2 have different interferograms under the left-handed and right-handed circular polarization incidences. Adapted with permission from [85]. © 2022 Wiley-VCH GmbH.

4.6. Plasmonic Tweezers and Particle Manipulation

Compared to optical tweezers (OTs), plasmonic tweezers (PTs) overcome the diffraction limit, offering a higher accuracy in particle manipulation. OTs, which rely on sufficient gradient forces, struggle to trap subwavelength-sized nanoparticles due to mismatches between the spot and particle sizes [86]. Additionally, trapping metal particles with OV tweezers is challenging due to the strong scattering force involved. To uncover the reason for the capability of PVs in trapping metal particles, Zhang et al. explored the trapping potential of metal particles with PV tweezers, finding that PV tweezers generated a dominant gradient force capable of counteracting the scattering force, thereby stabilizing particle trapping (Figure 13) [87].

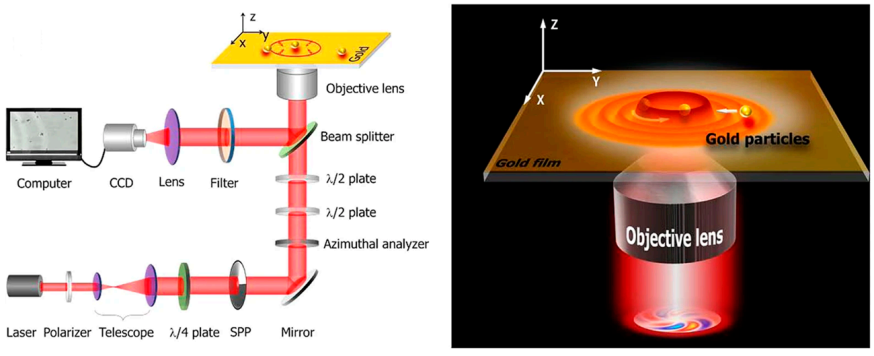

(**a**)

Figure 13. *Cont.*

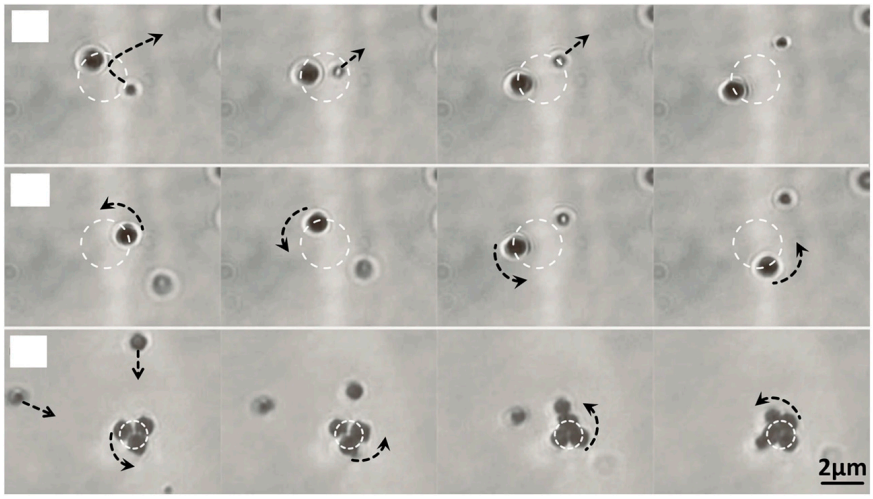

(**b**)

Figure 13. Plasmonic and optical spanner. (**a**) Schematic of the spanner setup and its conceptually operational principles, capable of stably trapping and dynamically rotating particles. (**b**) Video recordings illustrating the movement of gold particles in the OV field (top two rows) and in the PV field (bottom row). The black arrows denote motion direction of particles. Reprinted from [87]. Copyright © 2015, The Author(s). Creative Commons Attribution 4.0 International License.

To address the limitation of fixed nanostructures in modulating the PV field, Ju et al. proposed a method for generating a holographic plasmonic field, where incident light is modulated through a digital holographic algorithm to control the spot number, location, and topological charge of PVs. This approach enables the dynamic trapping and rotation of multiple gold particles [88]. Tsai et al., in contrast, used the plasmonic near-field generated by a gold plasmonic AS to selectively trap or rotate dielectric microparticles [89]. Later, Zaman et al. analyzed the three-dimensional optical force field produced by a plasmonic AS to further explain Tsai's results. They decomposed the force into conservative and solenoidal components and observed that the right-handed plasmonic AS generated a notable solenoidal force under right-handed, circularly polarized excitation, which induced the rotation of the trapped particle [86].

4.7. Electron Beam Shaping

A tailored electron beam holds good promise for applications such as nanolithography, microscopy, and imaging. Madan et al. employed an external spatial light modulator to import the desired amplitude and phase characteristics to a light field, which were then transferred to the electron beam via inelastic electron-light scattering on a flat, electron-transparent plate. This method works for both Hermite–Gaussian and LG modulations [90]. Recently, Huo et al. demonstrated the generation of structured electron vortex beams with customizable intensity patterns in free space using electron diffraction holography [91].

Moreover, these studies have broadened the scope of this field by inducing spatial electron modulation based on ultrafast interactions between electron pulses and plasmonic fields [92,93]. Vanacore et al. demonstrated this by using a femtosecond chiral plasmonic field generated by illuminating a circularly polarized pulsed laser onto a nanofabricated hole in a silver film on a Si_3N_4 membrane. This setup enables the interaction of both light and SPP fields with electron wavepackets as they pass through the hole, creating and controlling an ultrafast electron vortex beam [92]. Tsesses et al. dynamically controlled the electron beam by shaping the SPP patterns through various plasmonic coupling slits and by adjusting the SPP boundary conditions with different laser polarizations (Figure 14). Furthermore, by tuning the incident laser intensity and pulse width, and by post-selecting

specific electron energies after an interaction with guided SPPs, they could unlock another type of electron spatial modulation [93].

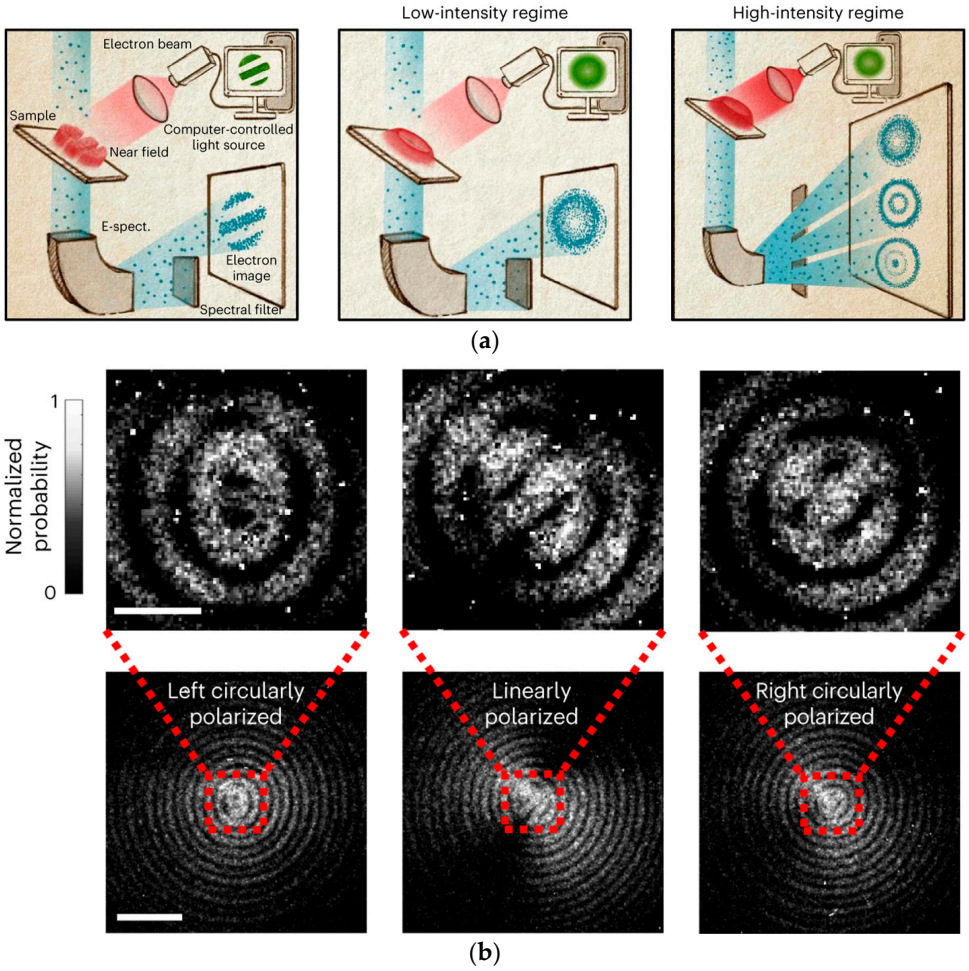

Figure 14. Free-electron spatial amplitude modulation. (**a**) Conceptual illustration of the modulation mechanism. (**b**) The spatial modulation of free electrons can be adjusted via altering the SPP field boundary conditions by changing the incident laser polarization. The upper scale bar, 10 μm; the lower scale bar, 0.5 μm. Reprinted with permission from [93]. Copyright © 2023, The Author(s), under exclusive license to Springer Nature Limited.

5. Conclusions

In this article, we reviewed three aspects of PVs: the generation and manipulation of PVs; the characterization of PVs; and the application of PVs. Although PVs have been studied intensively in the two most recent decades, more efforts are still needed to push PVs forward as a promising tool in both fundamental research and practical applications. For instance, we mentioned their potential application in chirality discrimination. However, the study mentioned in this review used ultrafast OAM light excitation, which complicates our understanding of the light–matter interaction in this process due to potential nonlinear effects. Thus, more work is still needed to explore the interaction mechanism involved and achieve chirality detection via pure PV excitation. Furthermore, their applications in super-resolution microscopy and spectroscopy warrant further exploration.

While significant breakthroughs have been made in the manipulation and characterization of PVs, leveraging their spatiotemporal characteristics remains an open challenge. It is already known that spin–orbit coupling plays a vital role in this process. However, how to use the process reversely remains an open question. Addressing this question

could deepen our understanding of light–matter interactions and expand their applications. Moreover, studies on controlling or shaping the spatiotemporal modulation of ultrafast PVs remain limited. We believe that insights from ultrafast optics and ultrafast plasmonics could provide valuable guidance in exploring this underdeveloped area. Some aspects, such as their dispersion behavior, interference process, and pulse manipulation, represent new frontiers that require further exploration. Regardless, we believe that PVs hold great potential for the future with continued dedicated efforts.

Author Contributions: Conceptualization, Z.G.; investigation, Z.G.; writing—original draft preparation, Z.G.; writing—review and editing, D.V.V., A.V.S. and Z.G.; supervision, A.V.S.; project administration, A.V.S.; funding acquisition, A.V.S. All authors have read and agreed to the published version of the manuscript.

Funding: This work was supported by the Robert A. Welch Foundation, grant number A-1547; the U.S. Department of Energy, Office of Science, Office of Biological and Environmental Research, grant number DE-SC-0023103; the U.S. Department of Energy, grant number DE-AC36-08GO28308 and grant number SUB-2023-10388.

Data Availability Statement: Not applicable.

Acknowledgments: Zhi Gao used GPT-3.5 to correct and modify English expressions and/or grammar for the draft.

Conflicts of Interest: The authors declare no conflicts of interest. The funders had no role in the design of the study; in the collection, analyses, or interpretation of data; in the writing of the manuscript; or in the decision to publish the results.

References

1. Allen, L.; Beijersbergen, M.W.; Spreeuw, R.J.C.; Woerdman, J.P. Orbital Angular Momentum of Light and the Transformation of Laguerre-Gaussian Laser Modes. *Phys. Rev. A* **1992**, *45*, 8185–8189. [CrossRef] [PubMed]
2. Willner, A.E.; Pang, K.; Song, H.; Zou, K.; Zhou, H. Orbital Angular Momentum of Light for Communications. *Appl. Phys. Rev.* **2021**, *8*, 041312. [CrossRef]
3. Lian, Y.; Qi, X.; Wang, Y.; Bai, Z.; Wang, Y.; Lu, Z. OAM Beam Generation in Space and Its Applications: A Review. *Opt. Lasers Eng.* **2022**, *151*, 106923. [CrossRef]
4. Pu, M.; Li, X.; Ma, X.; Wang, Y.; Zhao, Z.; Wang, C.; Hu, C.; Gao, P.; Huang, C.; Ren, H.; et al. Catenary Optics for Achromatic Generation of Perfect Optical Angular Momentum. *Sci. Adv.* **2015**, *1*, e1500396. [CrossRef] [PubMed]
5. Chen, J.; Wan, C.; Zhan, Q. Engineering Photonic Angular Momentum with Structured Light: A Review. *Adv. Photonics* **2021**, *3*, 064001. [CrossRef]
6. Shen, Y.; Wang, X.; Xie, Z.; Min, C.; Fu, X.; Liu, Q.; Gong, M.; Yuan, X. Optical Vortices 30 Years on: OAM Manipulation from Topological Charge to Multiple Singularities. *Light Sci. Appl.* **2019**, *8*, 90. [CrossRef] [PubMed]
7. Tu, Q.; Liu, J.; Ke, S.; Wang, B.; Lu, P. Directional Excitation of Surface Plasmon Polaritons by Circularly Polarized Vortex Beams. *Plasmonics* **2020**, *15*, 727–734. [CrossRef]
8. Ritchie, R.H. Plasma Losses by Fast Electrons in Thin Films. *Phys. Rev.* **1957**, *106*, 874–881. [CrossRef]
9. Liu, S.; Hou, Y.; Xie, W.; Schlücker, S.; Yan, F.; Lei, D.Y. Quantitative Determination of Contribution by Enhanced Local Electric Field, Antenna-Amplified Light Scattering, and Surface Energy Transfer to the Performance of Plasmonic Organic Solar Cells. *Small* **2018**, *14*, e1800870. [CrossRef] [PubMed]
10. Atwater, H.A.; Polman, A. Plasmonics for Improved Photovoltaic Devices. *Nat. Mater.* **2010**, *9*, 205–213. [CrossRef] [PubMed]
11. Wang, Z.; Chen, J.; Khan, S.A.; Li, F.; Shen, J.; Duan, Q.; Liu, X.; Zhu, J. Plasmonic Metasurfaces for Medical Diagnosis Applications: A Review. *Sensors* **2022**, *22*, 133. [CrossRef] [PubMed]
12. Zhan, C.; Yi, J.; Hu, S.; Zhang, X.-G.; Wu, D.-Y.; Tian, Z.-Q. Plasmon-Mediated Chemical Reactions. *Nat. Rev. Methods Primers* **2023**, *3*, 12. [CrossRef]
13. Anker, J.N.; Hall, W.P.; Lyandres, O.; Shah, N.C.; Zhao, J.; Van Duyne, R.P. Biosensing with Plasmonic Nanosensors. *Nat. Mater.* **2008**, *7*, 442–453. [CrossRef] [PubMed]
14. Shrivastav, A.M.; Cvelbar, U.; Abdulhalim, I. A Comprehensive Review on Plasmonic-Based Biosensors Used in Viral Diagnostics. *Commun. Biol.* **2021**, *4*, 70. [CrossRef] [PubMed]

15. Divya, J.; Selvendran, S.; Raja, A.S.; Sivasubramanian, A. Surface Plasmon Based Plasmonic Sensors: A Review on Their Past, Present and Future. *Biosens. Bioelectron. X* **2022**, *11*, 100175. [CrossRef]
16. Wang, M.; Wang, T.; Ojambati, O.S.; Duffin, T.J.; Kang, K.; Lee, T.; Scheer, E.; Xiang, D.; Nijhuis, C.A. Plasmonic Phenomena in Molecular Junctions: Principles and Applications. *Nat. Rev. Chem.* **2022**, *6*, 681–704. [CrossRef]
17. Xu, Q.; Lang, Y.; Jiang, X.; Yuan, X.; Xu, Y.; Gu, J.; Tian, Z.; Ouyang, C.; Zhang, X.; Han, J.; et al. Meta-Optics Inspired Surface Plasmon Devices. *Photonics Insights* **2023**, *2*, R02. [CrossRef]
18. Fang, Y.; Sun, M. Nanoplasmonic Waveguides: Towards Applications in Integrated Nanophotonic Circuits. *Light Sci. Appl.* **2015**, *4*, e294. [CrossRef]
19. Kristensen, A.; Yang, J.K.W.; Bozhevolnyi, S.I.; Link, S.; Nordlander, P.; Halas, N.J.; Mortensen, N.A. Plasmonic Colour Generation. *Nat. Rev. Mater.* **2016**, *2*, 16088. [CrossRef]
20. Wang, X.; Huang, S.-C.; Hu, S.; Yan, S.; Ren, B. Fundamental Understanding and Applications of Plasmon-Enhanced Raman Spectroscopy. *Nat. Rev. Phys.* **2020**, *2*, 253–271. [CrossRef]
21. Langer, J.; Jimenez de Aberasturi, D.; Aizpurua, J.; Alvarez-Puebla, R.A.; Auguié, B.; Baumberg, J.J.; Bazan, G.C.; Bell, S.E.J.; Boisen, A.; Brolo, A.G.; et al. Present and Future of Surface-Enhanced Raman Scattering. *ACS Nano* **2020**, *14*, 28–117. [CrossRef]
22. Pilot, R.; Signorini, R.; Durante, C.; Orian, L.; Bhamidipati, M.; Fabris, L. A Review on Surface-Enhanced Raman Scattering. *Biosensors* **2019**, *9*, 57. [CrossRef]
23. Lee, S.G.; Kwak, S.; Son, W.-K.; Kim, S.; Nam, K.T.; Lee, H.-Y.; Jeong, D.H. Chiral-Induced Surface-Enhanced Raman Optical Activity on a Single-Particle Substrate. *Anal. Chem.* **2024**, *96*, 9894–9900. [CrossRef] [PubMed]
24. Li, J.-F.; Li, C.-Y.; Aroca, R.F. Plasmon-Enhanced Fluorescence Spectroscopy. *Chem. Soc. Rev.* **2017**, *46*, 3962–3979. [CrossRef] [PubMed]
25. Lin, C.; Li, Y.; Peng, Y.; Zhao, S.; Xu, M.; Zhang, L.; Huang, Z.; Shi, J.; Yang, Y. Recent Development of Surface-Enhanced Raman Scattering for Biosensing. *J. Nanobiotechnol.* **2023**, *21*, 149. [CrossRef]
26. He, Q.; Zhang, Y.; Yang, Z.; Dong, J.; Lin, X.; Li, J. Surface-Enhanced Raman Spectroscopy: Principles, Methods, and Applications in Energy Systems. *Chin. J. Chem.* **2023**, *41*, 355–369. [CrossRef]
27. He, Z.; Han, Z.; Kizer, M.; Linhardt, R.J.; Wang, X.; Sinyukov, A.M.; Wang, J.; Deckert, V.; Sokolov, A.V.; Hu, J.; et al. Tip-Enhanced Raman Imaging of Single-Stranded DNA with Single Base Resolution. *J. Am. Chem. Soc.* **2019**, *141*, 753–757. [CrossRef]
28. Ohno, T.; Miyanishi, S. Study of Surface Plasmon Chirality Induced by Archimedes' Spiral Grooves. *Opt. Express* **2006**, *14*, 6285–6290. [CrossRef]
29. Gorodetski, Y.; Niv, A.; Kleiner, V.; Hasman, E. Observation of the Spin-Based Plasmonic Effect in Nanoscale Structures. *Phys. Rev. Lett.* **2008**, *101*, 043903. [CrossRef] [PubMed]
30. Tsai, W.-Y.; Sun, Q.; Hu, G.; Wu, P.C.; Lin, R.J.; Qiu, C.-W.; Ueno, K.; Misawa, H.; Tsai, D.P. Twisted Surface Plasmons with Spin-Controlled Gold Surfaces. *Adv. Opt. Mater.* **2019**, *7*, 1801060. [CrossRef]
31. Tan, Q.; Guo, Q.; Liu, H.; Huang, X.; Zhang, S. Controlling the Plasmonic Orbital Angular Momentum by Combining the Geometric and Dynamic Phases. *Nanoscale* **2017**, *9*, 4944–4949. [CrossRef]
32. Zhang, Y.; Zeng, X.; Ma, L.; Zhang, R.; Zhan, Z.; Chen, C.; Ren, X.; He, C.; Liu, C.; Cheng, C. Manipulation for Superposition of Orbital Angular Momentum States in Surface Plasmon Polaritons. *Adv. Opt. Mater.* **2019**, *7*, 1900372. [CrossRef]
33. Zang, X.; Zhu, Y.; Mao, C.; Xu, W.; Ding, H.; Xie, J.; Cheng, Q.; Chen, L.; Peng, Y.; Hu, Q.; et al. Manipulating Terahertz Plasmonic Vortex Based on Geometric and Dynamic Phase. *Adv. Opt. Mater.* **2019**, *7*, 1801328. [CrossRef]
34. Prinz, E.; Spektor, G.; Hartelt, M.; Mahro, A.-K.; Aeschlimann, M.; Orenstein, M. Functional Meta Lenses for Compound Plasmonic Vortex Field Generation and Control. *Nano Lett.* **2021**, *21*, 3941–3946. [CrossRef] [PubMed]
35. Shutova, M.; Quintero-Torres, R.; Kamble, M.; Sokolov, A.V. Gold Nanolens for Chiral Single Molecule Spectroscopy. *Laser Phys. Lett.* **2022**, *19*, 035701. [CrossRef]
36. Sunaba, Y.; Ide, M.; Takei, R.; Sakai, K.; Pin, C.; Sasaki, K. Nano-Shaping of Chiral Photons. *Nanophotonics* **2023**, *12*, 2499–2506. [CrossRef]
37. Wang, Y.; Zhao, P.; Feng, X.; Xu, Y.; Liu, F.; Cui, K.; Zhang, W.; Huang, Y. Dynamically Sculpturing Plasmonic Vortices: From Integer to Fractional Orbital Angular Momentum. *Sci. Rep.* **2016**, *6*, 36269. [CrossRef] [PubMed]
38. Zang, X.; Li, Z.; Zhu, Y.; Xu, J.; Xie, J.; Chen, L.; Balakin, A.V.; Shkurinov, A.P.; Zhu, Y.; Zhuang, S. Geometric Metasurface for Multiplexing Terahertz Plasmonic Vortices. *Appl. Phys. Lett.* **2020**, *117*, 171106. [CrossRef]
39. Huang, F.; Jiang, X.; Yuan, H.; Sun, X. Generation of Plasmonic Vortex with Linearly Polarized Light. *Plasmonics* **2017**, *12*, 751–757. [CrossRef]
40. Bai, Y.; Zhang, Q.; Yang, Y. Generation of Tunable Plasmonic Vortices by Varying Wavelength of Incident Light. *Photonics* **2022**, *9*, 809. [CrossRef]
41. Gu, K.; Zhang, Y.; Zhao, H.; Xu, B.; Ni, B.; Sun, M.; Liu, X.; Xiong, J. Manipulation of Plasmonic Vortex Fields Using Positive Elliptically Polarized Beams. *Opt. Laser Technol.* **2024**, *169*, 110132. [CrossRef]

42. Yuan, L.; Wang, J.; Wang, S.; Li, X.; Han, J.; Shen, X.; Hao, Z.-C.; Zhao, L. Localized Plasmonic Vortex Printing Technology Based on the Metaparticle and Spoof Surface Plasmon Polaritons. *Phys. Status Solidi A* **2021**, *218*, 2000708. [CrossRef]
43. Xu, Q.; Ma, S.; Hu, C.; Xu, Y.; Ouyang, C.; Zhang, X.; Li, Y.; Zhang, W.; Tian, Z.; Gu, J.; et al. Coupling-Mediated Selective Spin-to-Plasmonic-Orbital Angular Momentum Conversion. *Adv. Opt. Mater.* **2019**, *7*, 1900713. [CrossRef]
44. Gu, K.; Zhang, Y.; Zhao, H.; Sun, M.; Xu, B.; Ni, B.; Liu, X.; Xiong, J. Manipulating Plasmonic Vortex Based on Meta-Atoms with Four Rectangular Slits. *Opt. Express* **2023**, *31*, 39927–39940. [CrossRef] [PubMed]
45. Triolo, C.; Savasta, S.; Settineri, A.; Trusso, S.; Saija, R.; Agarwal, N.R.; Patanè, S. Near-Field Imaging of Surface-Plasmon Vortex-Modes around a Single Elliptical Nanohole in a Gold Film. *Sci. Rep.* **2019**, *9*, 5320. [CrossRef]
46. Ghanei, A.M.; Aghili, A.; Darbari, S.; Talebi, N. Plasmonic Vortices for Tunable Manipulation of Target Particles, Using Arrays of Elliptical Holes in a Gold Layer. *Sci. Rep.* **2023**, *13*, 54. [CrossRef] [PubMed]
47. Yang, Y.; Wu, L.; Liu, Y.; Xie, D.; Jin, Z.; Li, J.; Hu, G.; Qiu, C.-W. Deuterogenic Plasmonic Vortices. *Nano Lett.* **2020**, *20*, 6774–6779. [CrossRef]
48. Spektor, G.; Prinz, E.; Hartelt, M.; Mahro, A.-K.; Aeschlimann, M.; Orenstein, M. Orbital Angular Momentum Multiplication in Plasmonic Vortex Cavities. *Sci. Adv.* **2021**, *7*, eabg5571. [CrossRef]
49. Yuan, X.; Xu, Q.; Lang, Y.; Jiang, X.; Xu, Y.; Chen, X.; Han, J.; Zhang, X.; Han, J.; Zhang, W. Tailoring Spatiotemporal Dynamics of Plasmonic Vortices. *Opto-Electron. Adv.* **2023**, *6*, 220133. [CrossRef]
50. Yuan, X.; Xu, Q.; Lang, Y.; Yao, Z.; Jiang, X.; Li, Y.; Zhang, X.; Han, J.; Zhang, W. Temporally Deuterogenic Plasmonic Vortices. *Nanophotonics* **2024**, *13*, 955–963. [CrossRef]
51. Li, W.; Zhang, S.; Zhou, Z.; Fu, Y.; Zhang, Y.; Yuan, X.; Min, C. Spatiotemporal Modulation of Ultrafast Plasmonic Vortices with Spin–Orbit Coupling. *New J. Phys.* **2024**, *26*, 053011. [CrossRef]
52. Michaelis, J.; Hettich, C.; Mlynek, J.; Sandoghdar, V. Optical Microscopy Using a Single-Molecule Light Source. *Nature* **2000**, *405*, 325–328. [CrossRef] [PubMed]
53. Krenn, J.R.; Dereux, A.; Weeber, J.C.; Bourillot, E.; Lacroute, Y.; Goudonnet, J.P.; Schider, G.; Gotschy, W.; Leitner, A.; Aussenegg, F.R.; et al. Squeezing the Optical Near-Field Zone by Plasmon Coupling of Metallic Nanoparticles. *Phys. Rev. Lett.* **1999**, *82*, 2590–2593. [CrossRef]
54. Sandtke, M.; Kuipers, L. Slow Guided Surface Plasmons at Telecom Frequencies. *Nat. Photonics* **2007**, *1*, 573–576. [CrossRef]
55. Ghenuche, P.; Cherukulappurath, S.; Taminiau, T.H.; van Hulst, N.F.; Quidant, R. Spectroscopic Mode Mapping of Resonant Plasmon Nanoantennas. *Phys. Rev. Lett.* **2008**, *101*, 116805. [CrossRef]
56. Lahiri, B.; Holland, G.; Aksyuk, V.; Centrone, A. Nanoscale Imaging of Plasmonic Hot Spots and Dark Modes with the Photothermal-Induced Resonance Technique. *Nano Lett.* **2013**, *13*, 3218–3224. [CrossRef] [PubMed]
57. Stockman, M.I.; Kling, M.F.; Kleineberg, U.; Krausz, F. Attosecond Nanoplasmonic-Field Microscope. *Nat. Photonics* **2007**, *1*, 539–544. [CrossRef]
58. Carli, M.; Zilio, P.; Garoli, D.; Giorgis, V.; Romanato, F. Sub-Wavelength Confinement of the Orbital Angular Momentum of Light Probed by Plasmonic Nanorods Resonances. *Opt. Express* **2014**, *22*, 26302–26311. [CrossRef]
59. Hachtel, J.A.; Cho, S.-Y.; Davidson, R.B.; Feldman, M.A.; Chisholm, M.F.; Haglund, R.F.; Idrobo, J.C.; Pantelides, S.T.; Lawrie, B.J. Spatially and Spectrally Resolved Orbital Angular Momentum Interactions in Plasmonic Vortex Generators. *Light Sci. Appl.* **2019**, *8*, 33. [CrossRef] [PubMed]
60. Spektor, G.; Kilbane, D.; Mahro, A.K.; Frank, B.; Ristok, S.; Gal, L.; Kahl, P.; Podbiel, D.; Mathias, S.; Giessen, H.; et al. Revealing the Subfemtosecond Dynamics of Orbital Angular Momentum in Nanoplasmonic Vortices. *Science* **2017**, *355*, 1187–1191. [CrossRef] [PubMed]
61. Spektor, G.; Kilbane, D.; Mahro, A.K.; Hartelt, M.; Prinz, E.; Aeschlimann, M.; Orenstein, M. Mixing the Light Spin with Plasmon Orbit by Nonlinear Light-Matter Interaction in Gold. *Phys. Rev. X* **2019**, *9*, 021031. [CrossRef]
62. Dai, Y.; Zhou, Z.; Ghosh, A.; Mong, R.S.K.; Kubo, A.; Huang, C.-B.; Petek, H. Plasmonic Topological Quasiparticle on the Nanometre and Femtosecond Scales. *Nature* **2020**, *588*, 616–619. [CrossRef] [PubMed]
63. Bauer, T.; Davis, T.J.; Frank, B.; Dreher, P.; Janoschka, D.; Meiler, T.C.; Heringdorf, M.-J.M.Z.; Kuipers, L.; Giessen, H. Ultrafast Time Dynamics of Plasmonic Fractional Orbital Angular Momentum. *ACS Photonics* **2023**, *10*, 4252–4258. [CrossRef]
64. Zhang, M.; Wang, J.; Tian, Q. Tip-Enhanced Raman Spectroscopy Based on Plasmonic Lens Excitation and Experimental Detection. *Opt. Express* **2013**, *21*, 9414–9421. [CrossRef]
65. Gu, K.; Sun, M.; Zhang, Y. Tip-Enhanced Raman Spectroscopy Based on Spiral Plasmonic Lens Excitation. *Sensors* **2022**, *22*, 5636. [CrossRef]
66. Gu, K.; Zhao, H.; Sun, M.; Xu, B.; Ni, B.; Usman, M.; Liu, X.; Xiong, J. A Feasibility Study on Scanning Imaging of Tip-Enhanced Raman Spectroscopy Using a Spiral Plasmonic Lens. *Opt. Quant. Electron.* **2024**, *56*, 1274. [CrossRef]
67. Brullot, W.; Vanbel, M.K.; Swusten, T.; Verbiest, T. Resolving Enantiomers Using the Optical Angular Momentum of Twisted Light. *Sci. Adv.* **2016**, *2*, e1501349. [CrossRef]

68. Bégin, J.-L.; Jain, A.; Parks, A.; Hufnagel, F.; Corkum, P.; Karimi, E.; Brabec, T.; Bhardwaj, R. Nonlinear Helical Dichroism in Chiral and Achiral Molecules. *Nat. Photonics* **2023**, *17*, 82–88. [CrossRef]
69. Hachtel, J.; Davidson, R.; Chisholm, M.; Haglund, R.; Pantelides, S.; Cho, S.-Y.; Lawrie, B. Nano-Chirality Detection with Vortex Plasmon Modes. In Proceedings of the 2017 Conference on Lasers and Electro-Optics (CLEO), San Jose, CA, USA, 14–19 May 2017; pp. 1–2.
70. Karimi, E.; Schulz, S.A.; De Leon, I.; Qassim, H.; Upham, J.; Boyd, R.W. Generating Optical Orbital Angular Momentum at Visible Wavelengths Using a Plasmonic Metasurface. *Light Sci. Appl.* **2014**, *3*, e167. [CrossRef]
71. Chen, W.; Abeysinghe, D.C.; Nelson, R.L.; Zhan, Q. Experimental Confirmation of Miniature Spiral Plasmonic Lens as a Circular Polarization Analyzer. *Nano Lett.* **2010**, *10*, 2075–2079. [CrossRef] [PubMed]
72. Yang, S.; Chen, W.; Nelson, R.L.; Zhan, Q. Miniature Circular Polarization Analyzer with Spiral Plasmonic Lens. *Opt. Lett.* **2009**, *34*, 3047–3049. [CrossRef] [PubMed]
73. Zhang, J.; Guo, Z.; Li, R.; Wang, W.; Zhang, A.; Liu, J.; Qu, S.; Gao, J. Circular Polarization Analyzer Based on the Combined Coaxial Archimedes' Spiral Structure. *Plasmonics* **2015**, *10*, 1255–1261. [CrossRef]
74. Afshinmanesh, F.; White, J.S.; Cai, W.; Brongersma, M.L. An Integrated Plasmonic Polarimeter. In Proceedings of the CLEO: 2011—Laser Science to Photonic Applications, Baltimore, MD, USA, 1–6 May 2011; pp. 1–2.
75. Afshinmanesh, F.; White, J.S.; Cai, W.; Brongersma, M.L. Measurement of the Polarization State of Light Using an Integrated Plasmonic Polarimeter. *Nanophotonics* **2012**, *1*, 125–129. [CrossRef]
76. Garoli, D.; Zilio, P.; Gorodetski, Y.; Tantussi, F.; De Angelis, F. Beaming of Helical Light from Plasmonic Vortices via Adiabatically Tapered Nanotip. *Nano Lett.* **2016**, *16*, 6636–6643. [CrossRef] [PubMed]
77. Maccaferri, N.; Gorodetski, Y.; Garoli, D. Helical Light Emission from Plasmonic Vortices via Magnetic Tapered Tip. *J. Phys. Conf. Ser.* **2018**, *961*, 012001. [CrossRef]
78. Gorodetski, Y.; Zilio, P.; Ponzellini, P.; Ardini, M.; Zambrana-Puyalto, X.; Jacassi, A.; Calandrini, E.; Garoli, D. Efficient OAM Generation at the Nanoscale Level by Means of Plasmonic Vortex Lens. In Proceedings of the Plasmonics: Design, Materials, Fabrication, Characterization, and Applications XV, San Diego, CA, USA, 6–10 August 2017; Volume 10346, pp. 196–203.
79. Zilio, P.; Parisi, G.; Garoli, D.; Carli, M.; Romanato, F. Bilayer Holey Plasmonic Vortex Lenses for the Far Field Transmission of Pure Orbital Angular Momentum Light States. *Opt. Lett.* **2014**, *39*, 4899–4902. [CrossRef] [PubMed]
80. Garoli, D.; Zilio, P.; Gorodetski, Y.; Tantussi, F.; De Angelis, F. Optical Vortex Beam Generator at Nanoscale Level. *Sci. Rep.* **2016**, *6*, 29547. [CrossRef]
81. Prinz, E.; Hartelt, M.; Spektor, G.; Orenstein, M.; Aeschlimann, M. Orbital Angular Momentum in Nanoplasmonic Vortices. *ACS Photonics* **2023**, *10*, 340–367. [CrossRef]
82. Wang, H.; Zheng, T.; Yuan, Z.; Fang, Z. Plasmonic Spiral Nanostructure for Analyzing the Angular Momentum of Light. *IEEE Photonics J.* **2017**, *9*, 4800306. [CrossRef]
83. Liu, A.-P.; Xiong, X.; Ren, X.-F.; Cai, Y.-J.; Rui, G.-H.; Zhan, Q.-W.; Guo, G.-C.; Guo, G.-P. Detecting Orbital Angular Momentum through Division-of-Amplitude Interference with a Circular Plasmonic Lens. *Sci. Rep.* **2013**, *3*, 2402. [CrossRef]
84. Mei, S.; Huang, K.; Liu, H.; Qin, F.; Mehmood, M.Q.; Xu, Z.; Hong, M.; Zhang, D.; Teng, J.; Danner, A.; et al. On-Chip Discrimination of Orbital Angular Momentum of Light with Plasmonic Nanoslits. *Nanoscale* **2016**, *8*, 2227–2233. [CrossRef]
85. Lang, Y.; Xu, Q.; Chen, X.; Han, J.; Jiang, X.; Xu, Y.; Kang, M.; Zhang, X.; Alù, A.; Han, J.; et al. On-Chip Plasmonic Vortex Interferometers. *Laser Photonics Rev.* **2022**, *16*, 2200242. [CrossRef]
86. Zaman, M.A.; Padhy, P.; Hesselink, L. Solenoidal Optical Forces from a Plasmonic Archimedean Spiral. *Phys. Rev. A* **2019**, *100*, 013857. [CrossRef]
87. Zhang, Y.; Shi, W.; Shen, Z.; Man, Z.; Min, C.; Shen, J.; Zhu, S.; Urbach, H.P.; Yuan, X. A Plasmonic Spanner for Metal Particle Manipulation. *Sci. Rep.* **2015**, *5*, 15446. [CrossRef]
88. Ju, Z.; Ma, H.; Zhang, S.; Xie, X.; Min, C.; Zhang, Y.; Yuan, X. All-Optically Controlled Holographic Plasmonic Vortex Array for Multiple Metallic Particles Manipulation. *Opt. Lett.* **2023**, *48*, 6577–6580. [CrossRef]
89. Tsai, W.-Y.; Huang, J.-S.; Huang, C.-B. Selective Trapping or Rotation of Isotropic Dielectric Microparticles by Optical Near Field in a Plasmonic Archimedes Spiral. *Nano Lett.* **2014**, *14*, 547–552. [CrossRef]
90. Madan, I.; Leccese, V.; Mazur, A.; Barantani, F.; LaGrange, T.; Sapozhnik, A.; Tengdin, P.M.; Gargiulo, S.; Rotunno, E.; Olaya, J.-C.; et al. Ultrafast Transverse Modulation of Free Electrons by Interaction with Shaped Optical Fields. *ACS Photonics* **2022**, *9*, 3215–3224. [CrossRef]
91. Huo, P.; Yu, R.; Liu, M.; Zhang, H.; Lu, Y.; Xu, T. Tailoring Electron Vortex Beams with Customizable Intensity Patterns by Electron Diffraction Holography. *Opto-Electron. Adv.* **2024**, *7*, 230184. [CrossRef]

92. Vanacore, G.M.; Berruto, G.; Madan, I.; Pomarico, E.; Biagioni, P.; Lamb, R.J.; McGrouther, D.; Reinhardt, O.; Kaminer, I.; Barwick, B.; et al. Ultrafast Generation and Control of an Electron Vortex Beam via Chiral Plasmonic near Fields. *Nat. Mater.* **2019**, *18*, 573–579. [CrossRef] [PubMed]
93. Tsesses, S.; Dahan, R.; Wang, K.; Bucher, T.; Cohen, K.; Reinhardt, O.; Bartal, G.; Kaminer, I. Tunable Photon-Induced Spatial Modulation of Free Electrons. *Nat. Mater.* **2023**, *22*, 345–352. [CrossRef] [PubMed]